Polymer Bulletin 22, 95–101 (1989)

Polymer Bulletin

Crystallization behavior of low molecular mass isotactic poly(propylene) fractions

James J. Janimak and Stephen Z. D. Cheng*

Institute and Department of Polymer Science, College of Polymer Science and Polymer Engineering, University of Akron, Akron, OH 44325–3909, USA

Summary

The overall crystallization and linear crystal growth kinetics for the (monoclinic) α-form of low molecular mass isotactic poly(propylene) (i-PP) fractions have been studied. Two processes can be found for the overall crystallization study via differential scanning calorimetry (DSC). Based on the nucleation theory, both the half-life time of the first process in overall crystallization kinetics and the linear crystal growth data show two regime transitions, namely, regime I/II and II/III transitions.

Introduction

Crystallization anomalies in isotactic poly(propylene) (i-PP) have been extensively researched during the past two decades[1-10]. The existence of multiple crystal structural forms has been well-recognized, as well as the different morphologies, which is largely dependent upon crystallization conditions[11-16]. It has been found that for the linear crystal growth of i-PP, three crystallization regimes can be observed based on the nucleation theory[17-20]. On the other hand, it has also been reported recently that the overall crystallization rate of i-PP, which involves both nucleation and crystal growth steps, also shows the regime transition behavior (regime I/II)[8]. Similar observations have been reported in the cases of poly(3,3-dimethylthietane) fractions,[21] polyethylene[8] and poly(ethylene oxide)[8]. In this paper, we will discuss and compare both experimental results of the overall crystallization kinetics and the linear crystal growth rate for two i-PP low molecular mass fractions with MW=2,000 and 3,000.

Experimental

Materials. The i-PP fractions used in this study were kindly provided by Dr. H. N. Cheng of Hercules Inc., DE. The molecular characteristics are listed in Table I.

*To whom offprint requests should be sent

TABLE I. Characteristic Analysis of i-PP Fractions

Designation	Isotacticity	$\overline{Mn}$	$\overline{Mw}/\overline{Mn}$	Molecularlength[a]
i-PP2k	0.98	2,000	1.5	10.29
i-PP3k	0.98	3,000	1.5	15.43

a. The molecular length was calculated by $\overline{Mn}/[3*42.08/0.6495]$ (nm), where 3 represents the number of repeating units per turn in chain conformation in the crystalline state; 42.08 is the molecular mass of i-PP per mole, and 0.6495 nm is the c*-axis of i-PP monoclinic unit cell (α-form).

Differential Scanning Calorimetry (DSC). Measurements were performed on a Perkin-Elmer DSC2. Both temperature and heat flow scales were calibrated by following standard procedures. The isothermal crystallization experiments were studied.

Polarised Optical Microscopy (POM). A POM of Nikon Labophot-pol was used in conjunction with a Mettler hot stage (FP-52). The linear crystal growth rates of the i-PP fraction films were measured via the observation of spherulitic or axialitic growth prior to the appearance of impingement effects. The hot stage was also calibrated with standard sharp melting materials.

Results and Discussions

Overall Crystallization Kinetics. The isothermal kinetic data of i-PP overall crystallization reveal several peculiar anomalies. First, one observes two different structural formation kinetics with two Avrami exponents of n_1, and n_2. With increasing the crystallization temperature, both values remain virtually invariant, as listed in Tables II and III (only 30% of the data are shown in the Tables). For n_1, it ranges from 1.8 to 2.2, and for n_2, from 0.2 to 0.6. This would imply that principally the dimensionality of crystal growth during the initial stage of crystallization is primarily two-dimensional. It can be proven by the POM observation as shown in Figure 1. One can see the spherulitic texture when the whole unit lies down, or the axialite-like texture when upright. With increasing the crystallization temperature, the crystalline texture becomes primarily axialitic.

Of special interest is the time at which the transition between two different crystallization processes occur at almost constant crystallinities in the temperature range studied. This however, corresponds well near to the time of spherulitic impingement, indicating that the second crystallization process occurs at a more finer structural scale within the spherulites. In general, such reduced values of the Avrami exponent may arise due to non-negligible fractions of crystal nuclei, or change of growth rate during crystallization, in addition to lower dimensional growth[22].

Second, from Tables II and III, one can find that the times to attain 50% of the maximum crystallinity increases for both processes with

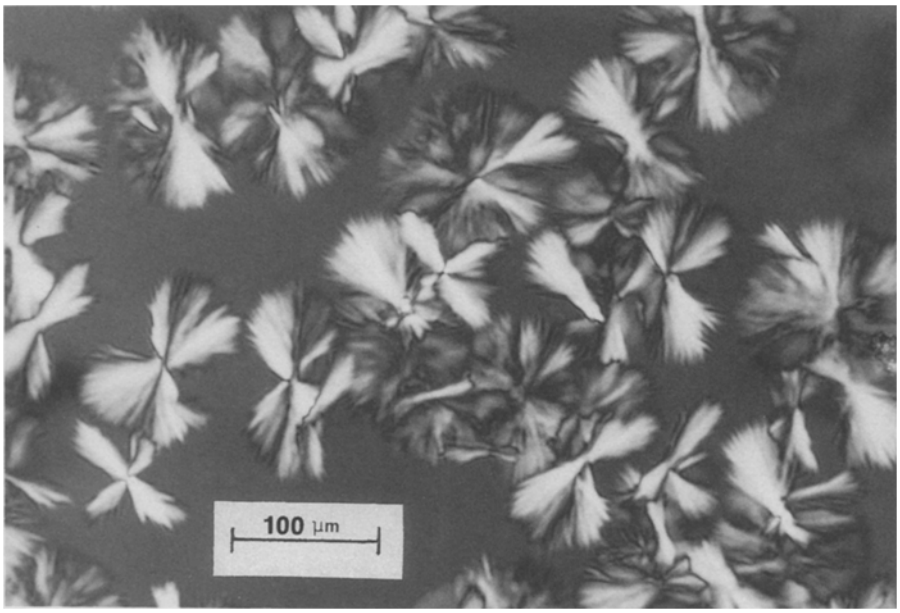

Figure 1. Crystalline morphology of i-PP3k at T_c=393.2k.

TABLE II. Overall Crystallization Data for i-PP2k

Tc(K)	n_1	n_2	K_1	K_2	$t_1(\frac{1}{2})$	$t_2(\frac{1}{2})$
347.2	1.83	0.272	0.144	-2.83	2.62	-0.900
353.2	2.42	0.331	3.27×10^{-2}	0.152	8.75	13.8
360.2	2.60	0.341	1.78×10^{-2}	0.226	14.9	9.0
370.2	1.84	0.552	3.42×10^{-3}	4.26×10^{-2}	1.10×10^{2}	29.4
380.2	1.76	0.266	1.18×10^{-4}	1.64×10^{-3}	1.72×10^{3}	1.58×10^{2}
390.2	1.95	0.352	5.61×10^{-5}	1.09×10^{-4}	2.64×10^{-5}	5.10×10^{4}

TABLE III. Overall Crystallization Data for i-PP3k

Tc(K)	n_1	n_2	K_1	K_2	$t_1(\frac{1}{2})$	$t_2(\frac{1}{2})$
349.2	1.81	0.227	0.271	0.800	1.41	3.81
358.2	1.80	0.808	7.97×10^{-2}	0.262	4.82	3.28
363.2	1.98	0.45	2.08×10^{-3}	0.137	16.9	11.1
373.2	2.23	0.32	7.22×10^{-4}	3.86×10^{-2}	4.31×10^{2}	56.2
384.2	1.94	0.67	4.03×10^{-5}	2.37×10^{-3}	8.85×10^{3}	4.35×10^{2}
394.2	1.80	0.48	1.11×10^{-6}	1.51×10^{-5}	6.25×10^{6}	9.45×10^{4}

increasing the crystallization temperature. Nevertheless, the time for the first process, $t_1(\frac{1}{2})$ increases much faster than that of the second process, $t_2(\frac{1}{2})$ since the first process represents an initial crystallization of i-PP molecules from the melt, and the second process may be largely related to a perfection process which is a solid state process[23].

A similar situation can also be found in the cases of rate constants, K_1 and K_2 in Tables II and III. However, since the physical origins of the rate constants are different from a solid state process to a liquid-solid transition, no quantitative comparison can be made. In contrast, for the first process, a dramatic decrease in the K_1 values with increasing the crystallization temperature indicate a change of nucleation density and linear crystal growth rate ($K=gNv^n$) with an almost constant geometric factor (g) and Avrami exponent (n).

Finally, it is obvious that at constant supercooling ($\Delta T=Tm^\circ-Tc$) the overall crystallization kinetics decreases with increasing molecular mass from MW=2,000 to 3,000 by adopting Tm°=425.2K for i-PP2k and 427.2K for i-PP3k[24]. Concentrating on only the half-life rates for both fractions, there is an almost 1.5 fold difference at ΔT=78K and the difference increases to about 10 fold at ΔT=35K.

Linear Crystal Growth Rate. Figure 2 shows the linear crystal growth rates of both fractions with respect to the crystallization temperature. It is quite obvious that there are two cross-over points for each fraction. This is clear indication that the different regime transitions are located at these cross-over points.

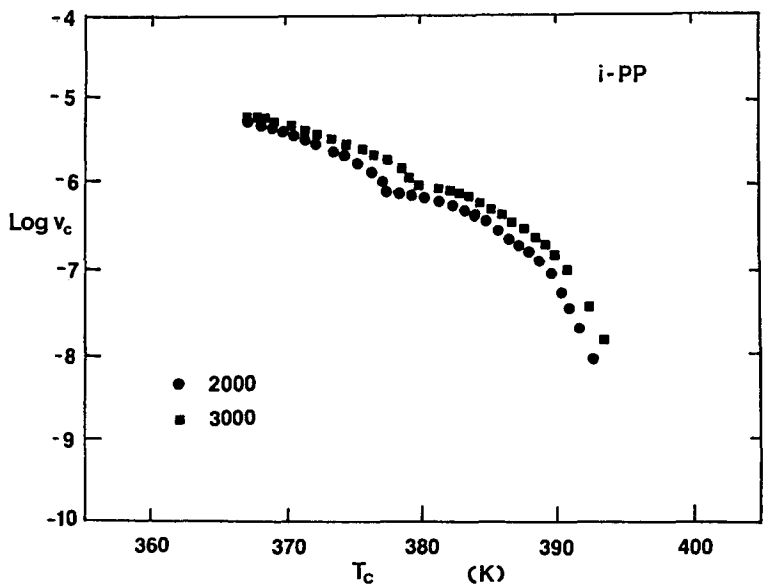

Figure 2. Relationship between the logarithmic crystal growth rate (log v_c) and crystallization temperature (Tc) for both i-PP2k (filled circles) and i-PP3k (filled square).

Regime Analyses. Based on the nucleation theory, one can plot the relationship between log v_c-log$\Delta T+U^*/[2.303(T_c-T_\infty)]$ and $1/[T_c(\Delta T)f]$, where v_c is the linear crystal growth rate, U* represents the activation energy (6.28kJ/mol), T_∞=Tg-30K, and $f=2T_c/(T_m^\circ+T_c)$. In order to treat the overall crystallization kinetics, the linear crystal growth rate, v_c, has to be replaced by the term, $[t_1(\frac{1}{2})]^{-1}$. Figure 3 shows the plots both for overall crystallization (top curve) and linear crystal growth rate (bottom curve) for i-PP2k. It is quite evident that both treatments show regime transition behavior at $\Delta T\tilde{=}48K$ (regime III/II transition) and $\Delta T\tilde{=}37K$ (regime II/I transition). Table IV lists the kinetic results for this fraction in both cases of overall crystallization and linear crystal growth data. The ratios of the slopes (K_g's) between neighboring regimes were found to be close to the theoretical prediction of two. Based on the relationship of $K_g(i)=n\sigma\sigma_e T_m^\circ/(k\Delta h_f)$ (when i=I and III, n=4; and i=II, n=2). The Δh_f is the heat of fusion per cubic centimeter, k is Boltzmann constant, and $\sigma\sigma_e$, the product of the lateral and fold surface free energies. From Figure 3, the values range between 1550 to 1750 erg^2/cm^4 from the analysis using linear crystal growth rates along the (110) growth plane. These values increase to 1800 to 2200 erg^2/cm^4 for the overall crystallization kinetics. Assuming a value of 11.5 erg/cm^2 for the lateral surface free energy, the fold surface free energy ranges between 137 - 150 erg/cm^2 for linear crystal growth rate measurements, and between 156-191 erg/cm^2 for overall crystallization kinetics, about 14-28% difference between these two treatments. Comparing with $\sim$70erg/cm^2 for the fold surface free energy of the folded chain crystals in the high molecular mass fractions, the higher fold surface free energy for i-PP2k is probably due to the short chain lengths (<11nm), which may form some degree of extended chain lamellar crystals with dangling chain ends in the melt. As a result, the fold surface free energy increases. Indeed, the equilibrium melting temperature of an intermediate molecular mass i-PP fraction (i-PP15k) makes a fold surface free energy of 247 erg/cm^2 when one calculates this free energy based on the melting temperature depression caused by the decrease of molecular mass[10]. However, the equilibrium melting temperature of i-PP fractions, especially its molecular mass dependence, are still largely uncertain. Additional experimental investigation is necessary for further discussion.

TABLE IV. Overall Crystallization and Linear Crystal Growth Kinetic Data of i-PP2k Fraction

Data Type	Regime	$K_g \times 10^5$ (k^{-2})	$\sigma\sigma_e$ (erg^2/cm^4)	Ratio[a]
Linear Crystal Growth Data	I	-2.825	1583	1.89
	II	-1.497	1678	2.06
	III	-3.083	1728	
Overall Crystallization Data	I	-3.277	1837	1.71
	II	-1.916	2148	1.91
	III	-3.660	2052	

a. The value of ratio between two neighboring regimes are $K_g(I)/K_g(II)$ and $K_g(III)/K_g(II)$.

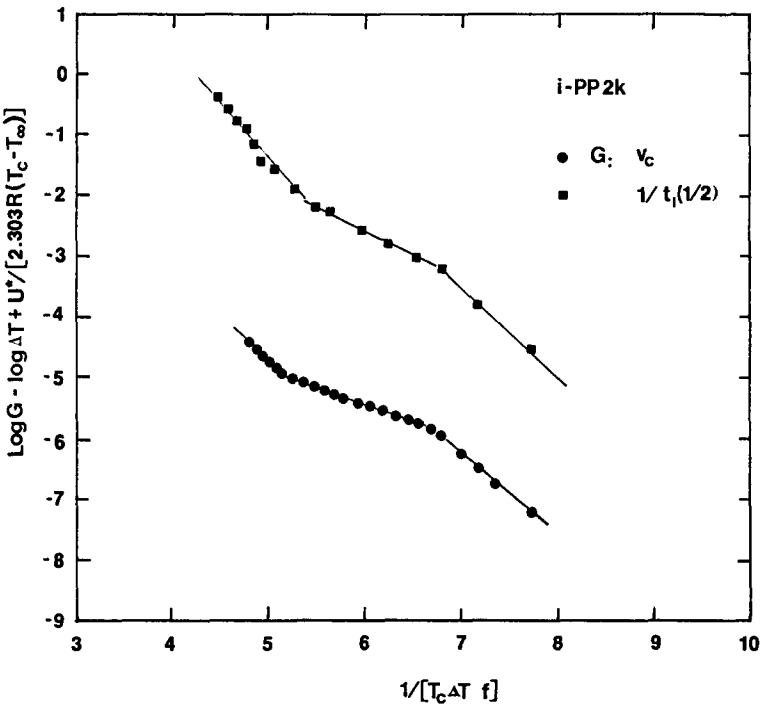

Figure 3. Plots of $\log [t(\frac{1}{2})]^{-1} - \log \Delta T + \frac{U^*}{[2.303\ R(T_c - T^\infty)]}$ (top curve)

and $\log v_c - \log \Delta T + \frac{U^*}{[2.303\ R(T_c - T^\infty)]}$ (bottom curve)

versus $1/[T_c(\Delta T)_f]$ for i-PP2k

References

1. F. J. Padden, Jr. and H. D. Keith, J. Appl. Phys. 1959, 30, 1479.
2. F. L. Binsbergen and B. G. M. deLange, Polymer 1970, 11, 309.
3. A. J. Lovinger, J. D. Chua, and L. C. Gryte, J. Polym. Sci. Polym. Phys. Ed. 1977, 15, 641.
4. L. Goldfarb, Makromol. Chem. 1978, 179, 2297.
5. A. Wlochowicz and M. Eder, Polymer 1981, 22, 1285.
6. E. Martuscelli, C. Silvestre, and G. Abate, Polymer 1982, 23, 229.
7. E. J. Clark and J. D. Hoffman, Macromolecules 1984, 17, 878.
8. R. C. Allen and L. Mandlekern, Polym. Bull. 1987, 17, 473.
9. R. A. Campbell, and P. J. Philips, Bull. Am. Phys. Soc. 1988, 33, 546; 989, 34, 754.
10. S. Z. D. Cheng, J. J. Janimak, A. Q. Zhang, and H. N. Cheng Macromolecules in press.
11. G. Natta and P. Corradini, Nuovo Cimento Supp. 1960, 15, 1.

12. H. D. Keith, F. J. Padden, Jr., N. M. Walter and M. W. Wycoff, J. Appl. Phys. 1959, 30, 1485.
13. G. DeRosa, R. Guerra, R. Napolitano, V. Petracone, and B. Pirozzi, Eur. Polym. J. 1984, 20, 937.
14. D. C. Bassett, and R. H. Olley Polymer 1984, 25, 935.
15. D. R. Norton, and A. Keller Polymer 1985, 26, 704.
16. H. Awaya Polymer 1988, 29, 591.
17. J. D. Hoffman, L. J. Frolen, G. R. Ross, and J. I. Lauritzen, Jr. J. Res. Natl. Bur. Std. 1975, 79A, 671.
18. J. I. Lauritzen, Jr. J. Appl. Phys. 1973, 44, 4353, see also J. I. Lauritzen, Jr., and J. D. Hoffman J. Appl. Phys. 1973, 44, 4340.
19. J. D. Hoffman, C. M. Guttman, and E. A. DiMarzio Discuss Faraday Chem. Soc. 1979, 68, 177.
20. J. D. Hoffman, Polymer 1982, 23, 656; 1983, 24, 3.
21. S. Lazcano, J. G. Fatou, C. Marco, and A. Bello Polymer 1988, 29, 2076.
22. S. Z. D. Cheng, and B. Wunderlich Macromolecules 1988, 21, 3327.
23. B. Wunderlich Macromolecular Physics, Vol. 2, Crystal Nucleation, Growth, Annealing. Academic Press, New York, 1976.
24. Unpublished extrapolated DSC data and small angle X-ray scattering measurements in our laboratory.

Accepted June 22, 1989 K